

Linearly aligned superradiant Bose-Einstein condensates diffracted by a single short laser pulse

Ichiro Inano, Keisuke Nakamura, and Atsuo Morinaga*

Faculty of Science and Technology, Tokyo University of Science, Noda-shi, Chiba 278-8510, Japan

(Received 31 August 2012; revised manuscript received 13 December 2012; published 23 April 2013)

Multiorder bidirectional superradiant Bose-Einstein condensates (BECs) were generated in a straight line by an irradiation of a single unidirectional short laser pulse along the long axis of a cigar-shaped sodium BEC in a magnetic trap. The probabilities of the diffracted BECs as a function of the laser intensity were well explained by the square of the Bessel functions and it was estimated that the intensity of the end-fire beam was 25% of the laser intensity. The backward diffractions disappeared at pulse duration longer than 5 μ s because of energy conservation. The probability for the + first-order diffraction grew exponentially with pulse duration when the backward diffractions disappeared. We observed the linearly aligned diffracted BECs along the propagation direction of the laser beam, regardless of the aspect ratio of the condensates. This fact indicates that the end-fire beam is triggered by the small backreflection from the vacuum window.

DOI: [10.1103/PhysRevA.87.043627](https://doi.org/10.1103/PhysRevA.87.043627)

PACS number(s): 03.75.-b, 37.10.Vz, 42.50.Gy

I. INTRODUCTION

Coherent matter-wave superradiance, which is the matter-wave analog of Dicke optical superradiance [1], is a promising tool for matter-wave amplification and matter-wave interferometry. The first discovery of a superradiance using a Bose-Einstein condensate (BEC) of ^{23}Na atoms was in 1999 [2], which was followed by many experimental studies [3–6] and theoretical studies of matter-wave superradiance [7–10]. In those experiments, when a single far-red-detuned, long laser pulse impinged along the short axis of a cigar-shaped BEC, multiple condensates with different momenta formed a highly regular and distinctive unidirectional scattering pattern spreading in the propagation direction of the laser. The observed matter-wave scattering pattern was explained as the result of spontaneous and stimulated Rayleigh superradiant scattering along the long axis (the so-called end-fire beam). Recently, the strong suppression of matter-wave superradiance using a blue-detuned pump laser was observed experimentally [11].

On the other hand, the diffraction of a matter wave by standing-wave light is well known as Kapitza-Dirac diffraction [12]. Gould *et al.* scattered a thermal atomic beam to several diffraction peaks of the forward and backward recoil momentum with even multiples by a near-resonant standing-wave laser field [13]. They showed that the probabilities of diffraction peaks are well described by Bessel functions with Rabi frequencies. Ovchinnikov *et al.* reported clear Kapitza-Dirac diffraction patterns using released sodium BECs with a pulsed standing-wave laser [14]. They observed periodic focusing and collimation of the condensates as a function of the pulse duration. Recently, the collapse and recurrence of the bidirectional momentum distribution and the matter-wave self-imaging were demonstrated using counterpropagating beams with a significant intensity difference [15]. Thus, it is established that the bidirectional momentum distributions are in good agreement with Bessel functions for relatively short-pulse duration in the standing-wave laser field [16,17].

Instead of the standing-wave laser, in 2003, Schneble *et al.* observed Kapitza-Dirac diffraction of superradiant atoms using a single short laser pulse along the short axis of a cigar-shaped ^{87}Rb BEC [18]. They proposed the explanation that the backward scattering of the atoms results from the reabsorption of spontaneously scattered photons (end-fire beam) and stimulated emission back into the pump beam. The end-fire beam and pump beam form an optical standing wave and diffracted atoms in a stimulated scattering process between momentum states. The qualitative difference in the diffraction patterns for the short- and long-pulse regimes is attributed to the transition from the Raman-Nath regime to the Bragg regime of diffraction, that is, to the onset of energy-momentum conservation for a sufficiently long interaction time. Subsequently, Pu *et al.* proposed a correlated pair production picture using four-wave mixing to correlate the backward- and forward-scattered atoms [19]. Deng and Hagley presented an analytical small-signal propagation theory on short-pulse, matter-wave superradiant scattering [20]. Such methods have been applied to realize coherent matter-wave amplifiers [21].

In this paper, the features of the superradiant BEC generated by the excitation of a single unidirectional short laser pulse are quantitatively investigated using sodium BECs with a relatively large number of atoms. The differences of this study compared to the previous study by Schneble *et al.* [18] are as follows: BECs are irradiated by a single circularly polarized laser pulse along the long axis of a cigar-shaped BEC [10,20], including a cold gas with an inversion shape from the cigar shape, before or after the release from a magnetic trap. The probabilities of superradiant BECs with different diffraction orders are measured as functions of the laser intensity, the pulse duration, the number of initial atoms in the BEC, and the time at which the irradiation takes place.

II. EXPERIMENTAL PROCEDURES

The experiments were performed with ^{23}Na condensates in the ground hyperfine $|S_{1/2}, F = 1, m_F = -1\rangle$ state, where F and m_F are the quantum numbers of the total spin and its z component, respectively. The experimental setup we used for creating BECs was similar to our previous setup

*morinaga@ph.noda.tus.ac.jp

[22]. Thermal sodium atoms were decelerated by a Zeeman slower and trapped by a dual-operation magneto-optical trap (MOT) [23], a temporal dark MOT, and a polarization gradient cooling. Next, the spin of the trapped atoms was polarized in the $|1, -1\rangle$ state using the spin-polarization technique [24] and cold atoms were captured directly in a compressed cloverleaf-type magnetic trap, whose trap frequencies were $\omega_r = 2\pi \times 173$ Hz and $\omega_z = 2\pi \times 21$ Hz. The horizontal z axis is the elongated axis of the condensates. Finally, by an rf-induced forced evaporative cooling for 30 s, a cigar-shaped ^{23}Na condensate was produced at the phase transition temperature of $1.2 \mu\text{K}$. We were able to produce BECs in the $|1, -1\rangle$ states, typically with 2.5×10^7 atoms and a density of 3×10^{14} atoms/cm³, every 3 min. The number of atoms in the condensate fluctuated by about 20% in each trial. The initial axial length of the condensate was about 0.3 mm and an aspect ratio of the axial length to the radial diameter was 8.5. After the release from the magnetic trap, the aspect ratio of the condensate decreased during the expansion, in accordance with the Thomas-Fermi approximation [25]. At a time of 9 ms after the release the shape was almost spherical and at a time of 21 ms after the release the aspect ratio was 0.5 and the pattern was reversed.

To generate superradiant scattering, the condensate was irradiated by a circularly polarized red-detuned laser pulse with a variable duration τ , which propagated along the z axis, at a time of T ms before or after the release from the magnetic trap. The typical pulse duration τ was $1 \mu\text{s}$. The detuning frequency of the laser was fixed to $\Delta/(2\pi) = -2.27$ GHz from the $S_{1/2}, |1, -1\rangle \rightarrow P_{3/2}, |2\rangle D_2$ transition at $\lambda = 589$ nm. The diameter of the laser beam was 3 mm and the beam intensity at its center I was changed from 1 to 590 mW/cm². The intensity of the laser beam backreflected from the window of the vacuum chamber was about 8% of that of the incident beam. (Even if the two laser beams reflected from the two surfaces of the window interfere constructively, the intensity is 16% at the maximum.) The window was located at 18 mm from the location of BECs. We aligned the laser beam carefully so that the reflection beam from the chamber window returned back at an angle more than 2° from the incident beam. Then the separation of the reflected beam and the incident beam was about 0.6 mm at the location

of BECs. As the released condensates moved downward, the position of the illumination was realigned.

To probe the momentum distribution of the scattered atoms, the horizontal spatial distribution of the atoms was observed using an absorption imaging method. After an additional time of flight (TOF), the condensates were optically pumped to the state $S_{1/2}, F = 2$ and were illuminated vertically by the probe beam, whose frequency was resonant to the transition from the $F = 2$ state to the $P_{3/2}, F' = 3$ state. The probe beam passed through BECs was detected using a charge-coupled device (CCD) camera with a spatial resolution of $10 \mu\text{m}$.

III. EXPERIMENTAL RESULTS

First, the pulse duration of the pump beam was fixed to $1 \mu\text{s}$. The condensates were irradiated by the pump beam at a time of 5 ms after the release from the magnetic trap, and absorption images were taken after an additional TOF of 9 ms. In Fig. 1 we present several images of the spatial distributions of BECs diffracted in a horizontal plane for different laser intensities. The laser beam propagates along the z axis, namely, from top to bottom in Fig. 1. As shown in Figs. 1(b)–1(e), with an increase of the laser intensity, a single condensate splits into several condensates, which are aligned in a straight line along the propagation direction of the laser pulse. We observed forward BECs with velocities parallel to the propagation direction of the pump beam and backward BECs with velocities antiparallel to that, which are symmetrical around the static condensate at the center. These condensates are called the plus or minus j th-order diffracted BECs and the original 0th-order condensate, respectively. We measured the velocities of the diffracted BECs by varying the TOF from 5 to 17 ms. As a result, the velocities were measured to be 12.4 ± 1.0 , 6.3 ± 0.7 , -6.6 ± 0.8 , and -12.8 ± 1.0 cm/s for the +second, +first, -first, and -second-order diffractions, respectively. Therefore, we could confirm that the diffracted BECs have a sodium recoil velocity of 2.9 cm/s multiplied by $2j$, namely $v = 2j\hbar k/M$ ($j = 1, 2, 3, \dots$), where k is the wave number of the pump beam and M is the mass of a sodium atom. In the present experiment, we used a σ^- circularly polarized light as the excitation pulse. However,

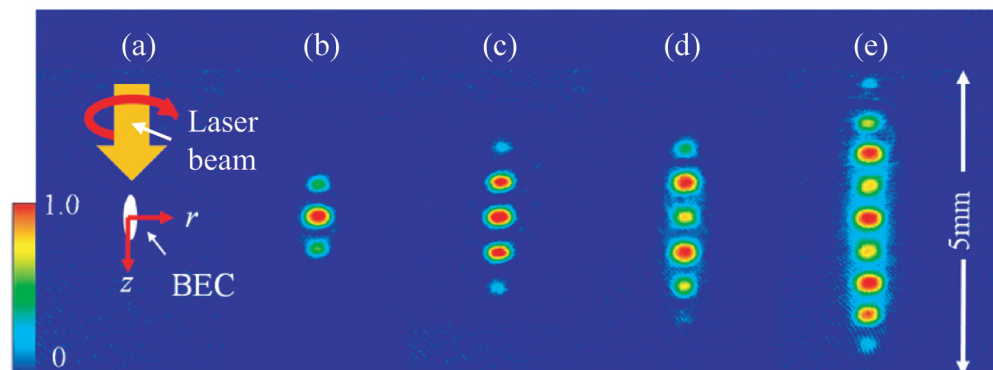


FIG. 1. (Color online) (a) Condensate is irradiated in a horizontal plane by a single circularly polarized short laser pulse with pulse duration of $1 \mu\text{s}$ propagating along the long axis (z axis) of the cigar-shaped sodium BEC at a time of 5 ms after the release from the magnetic trap. Absorption images (b)–(e) are taken after an additional TOF of 9 ms. Detuning frequency is 2.27 GHz. Laser intensities are (b) 26 mW/cm², (c) 130 mW/cm², (d) 260 mW/cm², and (e) 590 mW/cm².

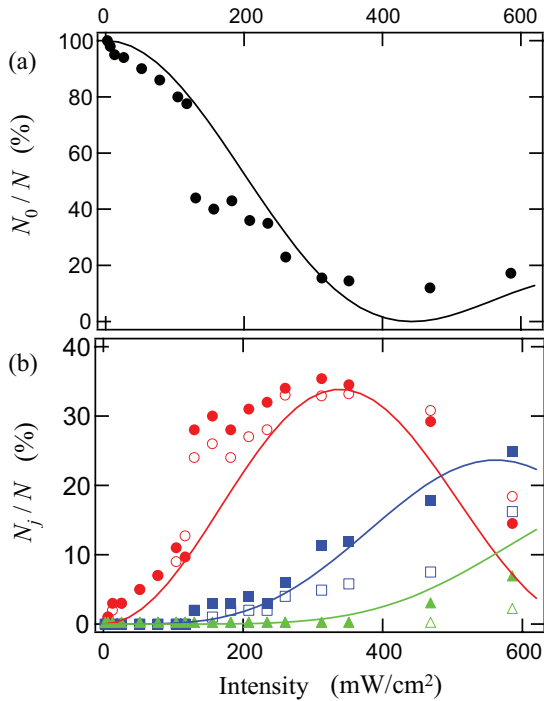


FIG. 2. (Color online) Probability of the diffracted condensates N_j/N versus laser intensity. (a) $j = 0$. Solid curve is the square of the Bessel function J_0^2 . (b) (\bullet) $j = +1$, (\circ) $j = -1$, (\blacksquare) $j = +2$, (\square) $j = -2$, (\blacktriangle) $j = +3$, and (\triangle) $j = -3$. Solid, dotted, and dashed curves are the square of the Bessel function of J_1^2 , J_2^2 , and J_3^2 , respectively. The dimensionless argument of the Bessel functions is $5.4 \times 10^{-3} I/(\text{mW}/\text{cm}^2)$, which were chosen to fit the data of $j = \pm 1$ and $+2$.

the probabilities for diffracted BECs did not change, even if we used a σ^+ circularly polarized light or linear polarized light. It was identified using the two-photon transitions that the diffracted BECs were almost in the $|1, -1\rangle$ state [26].

Figure 2 shows the probability of the j th-order diffracted BECs as a function of the laser intensity at pulse duration of $1 \mu\text{s}$. The probability P_j is the ratio of the number of atoms in the j th-order diffraction, N_j , on the number of atoms in the original condensate, N . The probability distributions of the diffracted BECs with $j = +1$ and $j = -1$ are almost the same over a span of intensities and they increase to a laser intensity of $350 \text{ mW}/\text{cm}^2$, then decrease at higher intensities, but that with $j = +2$ increases till $590 \text{ mW}/\text{cm}^2$. On the other hand, the probability of the 0th-order condensate decreases to $400 \text{ mW}/\text{cm}^2$ and increases again [see Fig. 1(e)]. It should be noted that the probability of the diffracted BECs with $j = -2$ (or -3) is smaller than that with $j = +2$ (or $+3$), although we will discuss this later. The dependence of N_j on the number of initial atoms in the condensate N was examined at a pulse duration of $1 \mu\text{s}$ and a fixed laser intensity of $200 \text{ mW}/\text{cm}^2$. The number of diffracted atoms for $j = +1$ and $+2$ was proportional to N , as shown in Fig. 3.

Next, the pattern of diffracted BECs was examined for different pulse duration τ at a weak intensity of the laser beam. The condensate was irradiated by a laser with an intensity of $13 \text{ mW}/\text{cm}^2$ at a time of 5 ms after the release, and

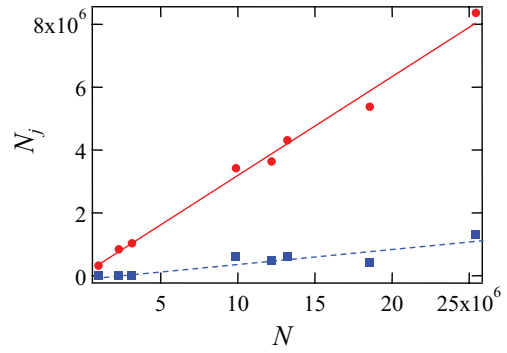


FIG. 3. (Color online) Number of atoms in the diffracted condensates for $j = 1$ (\bullet) and $j = 2$ (\blacksquare) versus the number of atoms in the condensate.

the absorption image was taken after an additional TOF of 13 ms . As shown in Fig. 4, with a $1\text{-}\mu\text{s}$ pump pulse, the diffracted BECs with $j = \pm 1$ were observed with the same weak probability; however, at $\tau = 3 \mu\text{s}$, the probability of $j = 1$ became greater than that of $j = -1$. At $5 \mu\text{s}$, the probability of $j = -1$ decreased. At $8 \mu\text{s}$, the diffracted BEC with $j = -1$ completely disappeared and that with $j = 1$ became more and more large. We examined the pattern for further pulse duration τ up to $70 \mu\text{s}$. We observed only the forward diffractions for $j = +1$ with almost the same probabilities for $j = 0$ and $j = 2$ with a small probability, but their patterns were smeared out and their numbers decreased as the pulse duration increased. Figure 5 shows the probabilities for $j = +1$ and $j = -1$ as a function of pulse duration up to $8 \mu\text{s}$.

Lastly, we examined the dependence of the diffracted patterns on the irradiation time T at which the irradiation takes place. The origin of T was defined as the moment that BECs were released from the magnetic trap. Figure 6 shows the absorption images for various T taken after an additional TOF of 13 ms . The intensity of the pulse was $200 \text{ mW}/\text{cm}^2$ and the pulse duration was $1 \mu\text{s}$. Figure 6(b) shows the diffracted BECs which were released from the magnetic trap immediately after irradiation of the pump beam ($T = 0$), as in the original experiment by Schneble *et al.* [18]. We see that the pattern of the diffractions becomes more distinctive when the BECs were irradiated by the pump beam after the release from the

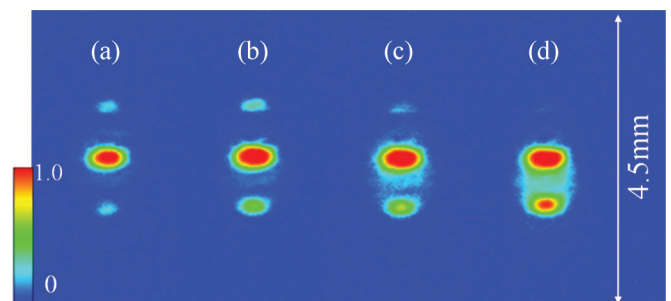


FIG. 4. (Color online) Diffraction pattern versus laser pulse duration. Laser beam with intensity of $13 \text{ mW}/\text{cm}^2$ propagates from top to bottom in the figure and condensates are irradiated at 5 ms after the release from the magnetic trap. Absorption images were taken after TOF of 13 ms . (a) Pulse duration of $1 \mu\text{s}$, (b) $3 \mu\text{s}$, (c) $5 \mu\text{s}$, and (d) $8 \mu\text{s}$.

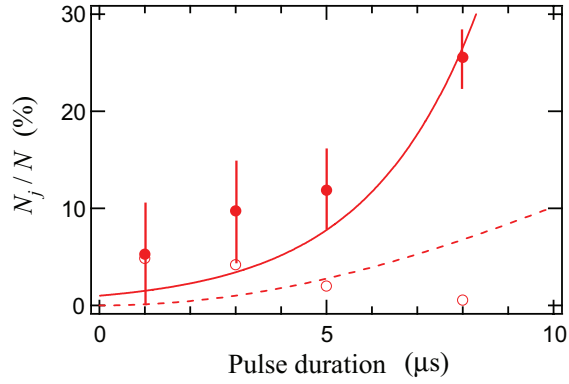


FIG. 5. (Color online) Probabilities for $j = 1$ (●) and $j = -1$ (○) versus laser pulse duration τ . Dashed curve is the square of the Bessel function $J_1^2(x)$ at $x = 0.070\tau/\mu\text{s}$. Solid curve is the exponential curve fitted to the data for $j = 1$.

magnetic trap. However, as shown in Fig. 7, the probability for $j = 1$ was almost constant ($\sim 32\%$) for any irradiation time.

IV. DISCUSSIONS

A. Pump beam intensity

It is known that the probability P_j of Kapitza-Dirac scattering in a standing wave is given by [13]

$$P_j = J_j^2[\Omega_1\Omega_2\tau/(2\Delta)], \quad (j = 0, \pm 1, \pm 2, \dots), \quad (1)$$

where J_j are Bessel functions of the first kind, Ω_1 and Ω_2 are the Rabi frequencies of two counterpropagating laser beams, τ is the pulse duration of the laser beam, and Δ is the detuning of the beams. The formula is valid on the assumption of $|\Delta| \gg \Omega_i$ and $\tau \ll \pi \Omega_i (|\Delta|\omega_r)^{1/2}$. The Rabi frequency is obtained from the laser intensity I_i using

$$\Omega_i = \Gamma \sqrt{I_i/(2I_s)}, \quad (2)$$

where Γ is the natural linewidth and I_s is the saturation intensity. In the case of a unidirectional laser excitation, Schneble *et al.* explained that the pump beam and the end-fire beam form an optical standing wave [18]. Therefore, we assume that the intensity of the end-fire beam as I_2 is proportional to the intensity of the pump beam $I_1 = I$ with

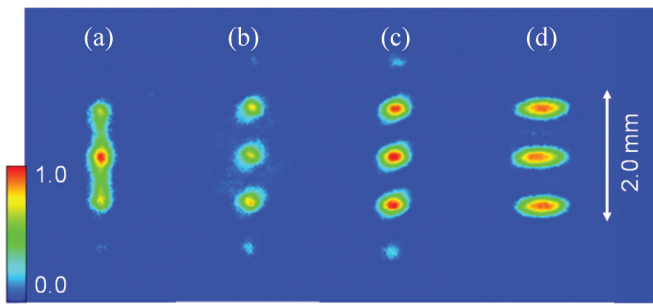


FIG. 6. (Color online) Diffraction pattern versus irradiation time T at which irradiation takes place after the release from the magnetic trap. Laser beam propagates from top to bottom in the figure. Pulse duration of laser is $1 \mu\text{s}$ and laser intensity is $200 \text{ mW}/\text{cm}^2$. Absorption images were taken after an additional TOF of 13 ms . (a) $T = -2 \text{ ms}$, (b) 0 ms , (c) 1 ms , and (d) 21 ms .

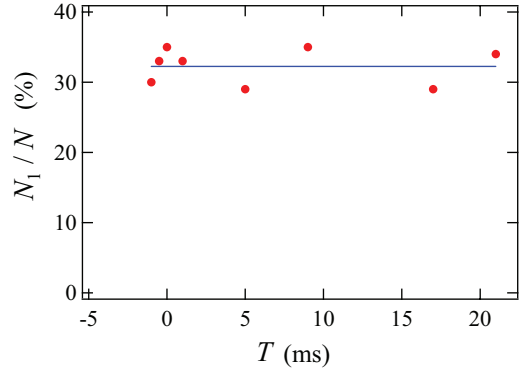


FIG. 7. (Color online) Probability of diffracted condensate of $j = 1$ as a function of the irradiation time T at which irradiation takes place after the release from the magnetic trap.

a proportional coefficient α . Then, the probability of the diffracted BECs is given by

$$P_j = J_j^2[\Gamma^2 \sqrt{\alpha} I \tau / (4\Delta I_s)]. \quad (3)$$

For the sodium D_2 transition, Γ is $2\pi \times 9.79 \text{ MHz}$ and I_s is $6.26 \text{ mW}/\text{cm}^2$ [27]. In the present experiment, the largest laser intensity used was about one hundred times the saturation intensity. However, the detuning frequency of $\Delta = 2.27 \text{ GHz}$ was sufficiently larger than the Rabi frequency, so that we could ignore the power broadening effect caused by the saturation. The measured probabilities of the diffracted BECs for $j = 0, \pm 1, +2$, and $+3$ were compared with the curves calculated using Eq. (3). When the proportional coefficient α is 0.25 , an overall coincidence between the experimental data and calculated curves were obtained without other scalable factors, as shown in Fig. 2(b), although the experimental probabilities for $j = \pm 1$ are somewhat larger than their calculated curves at the higher side of the intensities. Figure 2(a) shows the probability for $j = 0$, together with the curve of the square of the Bessel function for $j = 0$ with $\alpha = 0.25$. These coincidences confirm that the multiorder bidirectional diffractions occur also in the short unidirectional laser beam excitation, as well as the case of the standing wave.

The present results show that the intensity of the end-fire beam was 25% of that of the irradiation laser beam. Thus, the value of α is constant, not depending on the laser intensity. In the Rb experiment reported by Schneble *et al.*, the population in the $j = -2$ peak was 50% of that in the $j = -1$ peak at the intensity of $63 \text{ mW}/\text{cm}^2$, detuning of 420 MHz , and a pulse duration of $5 \mu\text{s}$ [18]. This means that the argument of the Bessel function is about 2.2 , so that we estimated that the α was roughly 0.05 , using Eq. (3) with the parameters of Rb [15]. Therefore, the present value is five times higher than that in the Rb experiment.

B. Pulse duration of pump beam

Li *et al.* reported that the multiorder bidirectional diffractions were observed in the short-pulse regime using the standing-wave laser with a strong beam and a weak counterpropagating beam, whose intensity was only 6% of the former one [15]. Therefore, the weak reflection beam from the chamber window ($\sim 8\%$) may form the standing wave with

the unidirectional pump beam in the present experiment. If it occurs, the multiorder bidirectional diffractions will collapse and reappear, and the matter-wave self-imaging will appear, as the pulse duration increases [15]. However, as shown in Fig. 4(e), the pattern for long pulse duration showed the unidirectional diffraction observed by Schneble *et al.* using a single traveling laser excitation [18]. We did not observe the revivals of the negative momentum distribution for pulse duration up to 70 μs . Thus, the reflection beam from the window did not form the standing wave.

The above experiments show that the transition from the Raman-Nath regime to the Bragg regime occurs as a function of the pulse duration. In sodium atoms excited by D_2 lines, the single-photon recoil frequency is $\omega_r = 1.5 \times 10^5 \text{ s}^{-1}$, which corresponds to a recoil time of $\omega_r^{-1} = 6.7 \mu\text{s}$, while the energy mismatch in the backward case is $8\hbar\omega_r$ [10]. Therefore, Kapitza-Dirac scattering can only take place when the energy uncertainty, $\hbar/\tau > 8\hbar\omega_r = 1.3 \times 10^{-28} \text{ J}$, is satisfied, that is, for pulse lengths of up to $\tau \sim 1 \mu\text{s}$. The emergence of this asymmetry at 5 μs in Fig. 4(c) is a clear signature for the transition from the Raman-Nath regime to the Bragg regime, that is, for the onset of energy conservation. For higher-order diffractions, the onset of energy conservation occurs at shorter pulse duration, so that the probability for $j = -2$ (or $j = -3$) was smaller than that for $j = +2$ (or $j = +3$), as shown in Fig. 2. Thus, we conclude that the atoms spontaneously emit photons along the propagation axis of the laser beam, which forms the end-fire beam whose energy is less than the energy of the pump beam.

C. Atom number of diffracted BEC

The experimental results of Fig. 2 show that the probability of diffracted BECs in the short laser pulse varies according to the Bessel function J_j . On the other hand, the number of the diffracted atoms N_j was proportional to the initial atom number of BEC in the condensate N , as shown in Fig. 3. Therefore, the number of atoms in the j th-order diffracted BECs are given by $N_j = NJ_j^2$. Thus, it was confirmed that the probability of the diffracted BECs is constant in the Raman-Nath regime.

Contradictorily, in the Bragg regime, Inouye *et al.* [2] suggested that the gain equation is

$$\dot{N}_j(t) = GN N_j(t). \quad (4)$$

Then the number of diffracted BECs grows exponentially as a function of pulse duration or the initial atom number N . This exponential growth of the diffraction probability for $j = 1$ is shown in Fig. 5, as a function of pulse duration. We can see that the probability for $j = +1$ grows as an exponential function (solid curve) much larger than the square of the Bessel function calculated using Eq. (3) (dashed curve), for the pulse duration more than 5 μs , while that for $j = -1$ decreases rapidly. Thus, the exponential growth of the probability for $j = 1$ starts when the diffracted BECs for $j = -1$ have disappeared because of energy conservation.

D. Irradiation time

The probabilities of the diffracted BECs for the different irradiation time T were almost constant, as shown in Fig. 7. Furthermore, the atoms for $j = \pm 1$ at $T = 21 \text{ ms}$ were still diffracted along the propagation direction of the pump beam, as shown in Fig. 6(d). When the pump is fired at this time, condensates expand due to the mean field energy and the density of atoms becomes very low. The aspect ratio of the condensate is inverted and the length of the BECs along the propagation axis of the laser beam becomes half of that along the radial axis. Without a pronounced aspect ratio and reflection of the pump beam, the scattered photons go in all directions. Therefore, the present result seems to be contradictory to known superradiant scattering theory that the end-fire beam is generated along the long axis of the condensates [2,18]. However, the fact that the scattering is still in the direction of the pump beam indicates to us that the end-fire beam is primarily triggered by the small backreflection from the vacuum window, and the probabilities of the diffracted BECs indicates that the end-fire beam grows up to 25% of the intensity of the pump beam. Thus, the diffraction observed using a cold gas with a low density will be superradiant scattering caused by the presence of a small backreflection.

V. CONCLUSION

In conclusion, we have examined quantitatively Kapitza-Dirac superradiant BECs aligned in a straight line induced by a single unidirectional short-pulse excitation, using a relatively large number of sodium BECs. Symmetrical multiorder backward- and forward-diffracted BECs are generated as the laser intensity increases. The probabilities of the diffracted BECs were well explained by the square of the Bessel functions, and it was deduced that the intensity of the end-fire beam was 25% of the laser intensity. The disappearance of the backward diffraction for pulse duration more than 5 μs is a clear signature for the transition from the Raman-Nath regime to the Bragg regime, that is, for the onset of energy conservation. This is proof that the superradiances observed in the present experiment occur in the unidirectional laser in the excitation. The exponential growth of the probability for the +first-order diffraction starts when the diffracted BECs for $j = -1$ disappeared because of energy conservation. The pattern and probability of the diffracted BECs did not change at different times at which the irradiation takes place.

At present, we are attempting to compose an atom interferometer using longitudinally aligned BECs which are irradiated by multiple short laser pulses.

ACKNOWLEDGMENT

We are grateful to Dr. Hiromitsu Imai and Koichi Toriyama for their observation of the linearly aligned superradiant BECs.

[1] R. H. Dicke, *Phys. Rev.* **93**, 99 (1954).

[2] S. Inouye, A. P. Chikkatur, D. M. Stamper-Kurn, J. Stenger, D. E. Pritchard, and W. Ketterle, *Science* **285**, 571 (1999).

[3] S. Inouye, T. Pfau, S. Gupta, A. P. Chikkatur, A. Görlitz, D. E. Pritchard, and W. Ketterle, *Nature* **402**, 641 (1999).

- [4] S. Inouye, R. F. Löw, S. Gupta, T. Pfau, A. Görlitz, T. L. Gustavson, D. E. Pritchard, and W. Ketterle, *Phys. Rev. Lett.* **85**, 4225 (2000).
- [5] M. Kozuma, L. Deng, E. W. Hagley, J. Wen, R. Lutwak, K. Helmerson, S. L. Rolston, and W. D. Phillips, *Phys. Rev. Lett.* **82**, 871 (1999).
- [6] Y. Yoshikawa, T. Sugiura, Y. Torii, and T. Kuga, *Phys. Rev. A* **69**, 041603(R) (2004).
- [7] M. G. Moore and P. Meystre, *Phys. Rev. Lett.* **83**, 5202 (1999).
- [8] Ö. E. Müstecaplioglu and L. You, *Phys. Rev. A* **62**, 063615 (2000).
- [9] N. Piovella, M. Gatelli, and R. Bonifacio, *Opt. Commun.* **187**, 165 (2001).
- [10] L. Deng, M. G. Payne, and E. W. Hagley, *Phys. Rev. Lett.* **104**, 050402 (2010).
- [11] L. Deng, E. W. Hagley, Q. Cao, X. Wang, X. Luo, R. Wang, M. G. Payne, F. Yang, X. Zhou, X. Chen, and M. Zhan, *Phys. Rev. Lett.* **105**, 220404 (2010).
- [12] P. L. Kapitza and P. A. M. Dirac, *Proc. Cambridge Philos. Soc.* **29**, 297 (1933).
- [13] P. L. Gould, G. A. Ruff, and D. E. Pritchard, *Phys. Rev. Lett.* **56**, 827 (1986).
- [14] Yu. B. Ovchinnikov, J. H. Müller, M. R. Doery, E. J. D. Vredenbregt, K. Helmerson, S. L. Rolston, and W. D. Phillips, *Phys. Rev. Lett.* **83**, 284 (1999).
- [15] K. Li, L. Deng, E. W. Hagley, M. G. Payne, and M. S. Zhan, *Phys. Rev. Lett.* **101**, 250401 (2008).
- [16] B. Gadway, D. Petrot, R. Reimann, M. G. Cohen, and D. Schneble, *Opt. Express* **17**, 19173 (2009).
- [17] S. Beattie, B. Barrett, I. Chan, C. Mok, I. Yavin, and A. Kumarakrishnan, *Phys. Rev. A* **80**, 013618 (2009).
- [18] D. Schneble, Y. Torii, M. Boyd, E. W. Streed, D. E. Pritchard, and W. Ketterle, *Science* **300**, 475 (2003).
- [19] H. Pu, W. Zhang, and P. Meystre, *Phys. Rev. Lett.* **91**, 150407 (2003).
- [20] L. Deng and E. W. Hagley, *Phys. Rev. A* **82**, 053613 (2010).
- [21] D. Schneble, G. K. Campbell, E. W. Streed, M. Boyd, D. E. Pritchard, and W. Ketterle, *Phys. Rev. A* **69**, 041601(R) (2004).
- [22] H. Imai and A. Morinaga, *J. Phys. Soc. Jpn.* **79**, 094005 (2010).
- [23] H. Tanaka, H. Imai, K. Furuta, Y. Kato, S. Tashiro, M. Abe, R. Tajima, and A. Morinaga, *Jpn. J. Appl. Phys.* **46**, L492 (2007).
- [24] K. M. R. van der Stam, A. Kuijk, R. Meppelink, J. M. Vogels, and P. van der Straten, *Phys. Rev. A* **73**, 063412 (2006).
- [25] F. Dalfovo, S. Giorgini, L. P. Pitaevski, and S. Stringari, *Rev. Mod. Phys.* **71**, 463 (1999).
- [26] H. Imai, T. Akatsuka, T. Ode, and A. Morinaga, *Phys. Rev. A* **85**, 013633 (2012).
- [27] D. A. Steck, Sodium D Line Data, <http://steck.us/alkalidata> (2010).